Non-permanent Pole-to-pole Fault Restoration Strategy for Flexible DC Distribution Network

Zainan Li, Jiandong Duan, Wenchao Lu, Xiaotong Du, Wei Yang, and Siyu Tu

Abstract—As the structures of multiple branch lines (MBLs) will be widely applied in the future flexible DC distribution network, there is a urgent need for improving system reliability by tackling the frequent non-permanent pole-to-pole (P-P) fault on distribution lines. A novel fault restoration strategy based on local information is proposed to solve this issue. The strategy firstly splits a double-ended power supply network into two single-ended power supply networks through the timing difference characteristics of a hybrid direct current circuit breaker (HDC-CB) entering the recloser. Then, a method based on the characteristic of the transient energy of fault current is proposed to screen the faulty branch line in each single-ended power supply network. Also, a four-terminal flexible DC distribution network with MBLs is constructed on PSCAD to demonstrate the efficacy of the proposed strategy. Various factors such as noise, fault location, and DC arc equivalent resistance are considered in the simulation model for testing. Test results prove that the proposed strategy for fault restoration is effective, and features high performance and scalability.

Index Terms—Flexible DC distribution network, pole-to-pole fault, fault restoration strategy, reclosing strategy, transient energy of fault current.

I. INTRODUCTION

THE Chinese government has proposed to reach a carbon peak by 2030 and carbon neutrality by 2060 [1]. To achieve this goal, the share of renewable energy is increasing at an accelerated rate. DC distribution networks have the following advantages: easy connection to distributed renewable energy sources [2], low losses [3], and high power quality [4] providing a strong guarantee for the consumption of renewable energy [5].

Unlike the AC distribution network, faults on the DC line cause more serious consequences. Insulated gate bipolar transistors (IGBTs) in the multi-module multi-level converter (MMC) are subjected to high fault current, increasing their probability of damage [6]. The technology for dealing with DC faults, mainly including DC line protection and DC fault isolation, has become mature gradually. DC overhead lines have already been widely used in various flexible DC system scenarios due to their economic advantages. Considering the fact that the fault probability on overhead lines is much higher, especially the non-permanent fault (NPF), fault restoration strategies need to be investigated to improve the reliability of the power supply network. Thus, this paper focuses on the NPF restoration strategy in overhead line scenarios.

The key of traditional fault restoration is to reliably determine the fault property (permanent fault (PF) or NPF) [7]. Reference [8] proposes a fault property screening scheme based on line voltage characteristics. The residual voltage characteristics of PFs and NPFs are analyzed in [9]. And a reclosing strategy is proposed for a direct current circuit breaker (DCCB) to reduce the probability of equipment being damaged in the system. The same logic scheme can also be applied to mechanical DCCBs [10]. In [11], a sequential switching strategy is proposed for hybrid DCCBs (HDC-CBs), which effectively reduces the peak fault current, overvoltage, and fault clearance time. For pole-to-ground (P-G) faults, with the help of coupling ideas, [12] proposes a fault restoration strategy for the fault-based induction voltage. The PF and NPF can be correctly judged during the fault restoration process. In [13], an auxiliary circuit is added to the HDCCB to identify the fault property during the fault restoration phase by discharging the capacitor inside the auxiliary circuit. With the MMC treated as a vehicle, the advantages offered by its high controllability are fully exploited. A new adaptive reclosing scheme is given in [14]. The scheme points out that during the fault restoration phase, the MMC injects a signal into the line. The fault property and fault location can both be determined by the travelling wave detection. In [15], a fault restoration strategy based on the signal injection method is proposed, which is applied to a P-G fault. The signal is injected into the non-faulty pole, and the fault property is identified by detecting the characteristic signal on the faulty line.

For the distribution network, a large number of distributed loads are often configured, and the structures of MBLs are required to meet the demand [16], [17]. The DC distribution networks with MBLs need to pay attention to fault restoration strategies, which can distinguish the fault property and

identify the faulty branch lines. The above-mentioned fault restoration strategies have made a lot of contributions from different perspectives, but they cannot be applied to the scenarios with MBLs. Consequently, a fault restoration strategy for the structures of MBLs is proposed, which has the function of identifying faulty branch lines.

There are two fault categories on DC lines: P-G fault and pole-to-pole (P-P) fault. Under the same system condition, a P-P fault usually results in a higher fault current, which could potentially cause more damages to the system. Therefore, the fault restoration strategy proposed in this paper mainly focuses on the P-P faults.

The main contributions of this paper are as follows.

1) The proposed strategy can distinguish the fault property (PF or NPF) and the DC line fault type (P-G or P-P), and identify specific faulty branch lines.

2) The proposed strategy is suitable for the scenarios with MBLs and is more suitable for distribution networks.

3) The proposed strategy is based on local information and does not need communication. It can be used as a backup for the communication-based fault restoration strategy.

4) The proposed strategy can be used in conjunction with other fault restoration strategies to provide a better fault restoration effect for the system.

The rest of this paper is organized as follows. In Section II, the topology of the flexible DC distribution network and the wavelet transform (WT) algorithm are analyzed. In Section III, a novel fault restoration strategy is proposed for P-P faults, which is based on the split method to construct an independent radiation network. The complete scheme of the proposed fault restoration strategy is given in Section IV. In Section V, the simulation model is established, and the performance of the proposed restoration strategy is evaluated under different fault conditions. Finally, the conclusions and potential limitations are presented in Section VI.

II. TOPOLOGY OF FLEXIBLE DC DISTRIBUTION NETWORK AND WT ALGORITHM

A. Topology of Flexible DC Distribution Network

In China, the need for MBLs has been demonstrated, especially by the operation of relevant DC projects [18]. Considering stability and fault restoration, current-limiting reactors (CLRs) are usually installed at the outlet of the MMC, which also means that CLRs are not configured between MBLs [19]. The diagram of a flexible DC distribution network with MBLs is shown in Fig. 1.
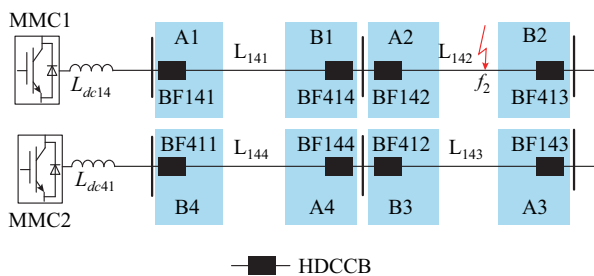

Fig. 1.   Diagram of a flexible DC distribution network with MBLs.

The distribution network shown in Fig. 1 is mainly used in urban power supply scenarios. The domestic urban load density is growing at a high rate. Taking Shanghai, China as an example, the current load density has reached 40 MW/km^2 [20]. To meet the load demand, ±100 kV is chosen as the supply voltage level [21]. Meanwhile, HDCCB is utilized in conjunction with protection schemes to remove faulty lines. The line between MMC1 and MMC2 is split into four branch lines, L_{141}, L_{142}, L_{143}, and L_{144}. To facilitate the analysis, each branch line has the same length. The line is further divided into eight areas, i.e., A1-A4 and B1-B4. The protection devices in each zone are calculated by the protection algorithm to give a trip command to the corresponding HDCCB. L_{dc14} and L_{dc41} are the CLRs used to limit the rate and amplitude of change of the fault current.

Considering that the communication of the protection device may fail, the protection device will not work normally. It is necessary to configure single-ended protection (no communication) as a backup for the pilot protection. Aiming at the frequent transient faults of overhead lines, our research group has studied a single-ended protection scheme suitable for the full cycle of the fault. The scheme is divided into two steps. ① Fault detection: build boundary fast protection with the help of CLRs, and issue trip instructions to HDCCB in areas A1 and B4. ② Fault restoration: judge the fault property (PF or NPF) and specific faulty lines. A large amount of literature focuses on fault detection, but the research on fault restoration is merely investigated.

The traditional fault restoration strategies can only judge the fault property and cannot determine faulty lines in MBL situations. For this paper, a novel fault restoration strategy for the flexible DC distribution network with MBLs is proposed, which aims to accurately identify faulty lines.

B. Fault Characteristic Analysis

When a P-P fault occurs on f_2 in L_{142}, the equivalent circuit of the fault loop is illustrated in Fig. 2, where L_{line} and R_{line} are the equivalent inductance and resistance of the faulty line, respectively; R_{on} is the equivalent resistance when the sub-module of the MMC is switched on; L_{arm} is the equivalent arm inductance of MMC; C is the equivalent capacitor of a sub-module; C_{MMC}, L_{MMC}, and R_{MMC} are the equivalent capacitance, inductance, and resistance of the MMC, respectively; N is the number of bridge arm sub-modules; and i is the line fault current. Meanwhile, the capacitor in the sub-module of the MMC quickly discharges to the fault point, and the equivalent circuit is composed of the MMC and lines. The line fault current can be expressed as:
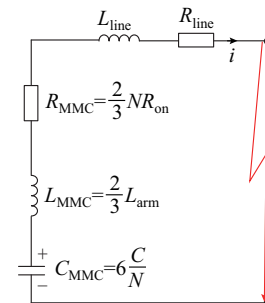

Fig. 2.   Equivalent circuit of fault loop when a P-P fault occurs.

$$i = A\sqrt{C_\Sigma/L_\Sigma}\, e^{-\sigma t} \sin(\omega t + \theta - \beta) \qquad (1)$$

$$\begin{cases} \sigma = R_\Sigma/(2L_\Sigma) \\ \theta - \beta = \arcsin(I_{load}/(A\sqrt{C_\Sigma/L_\Sigma})) \\ A = \sqrt{U_{dc}^2 + [U_{dc}\sigma/\omega - I_{load}/(\omega C_\Sigma)]^2} \\ R_\Sigma = R_{MMC} + R_{line} \\ L_\Sigma = L_{MMC} + L_{line} \\ C_\Sigma = C_{MMC} \end{cases} \qquad (2)$$

where U_{dc} and I_{load} are the DC rate voltage and rate current; A is the variable coefficient; σ is the time constant of the fault loop; ω is the grid angular frequency; θ is the initial phase angle before failure; and $\theta - \beta$ is the initial phase angle after a fault.

The equivalent circuit shown in Fig. 2 is an RLC second-order oscillation circuit, and the oscillation frequency of the fault current can be expressed as:

$$f_o = \frac{\sqrt{[(L_{MMC} + L_{line})C_{MMC}]^{-1} - \{R_{Line}/[2(L_{MMC} + L_{line})]\}^2}}{2\pi} \qquad (3)$$

In general, $[(L_{MMC} + L_{line})C_{MMC}]^{-1}$ is much greater than $\{R_{line}/[2(L_{MMC} + L_{line})]\}^2$, so the frequency of the current is mainly restricted by $[(L_{MMC} + L_{line})C_{MMC}]^{-1}$.

Taking a demonstration project as an example, we assume $L_{arm} = 15$ mH, $C = 600$ μF, and $N = 4$. A P-P fault occurs at the outlet side of the MMC, and the f_o corresponding to the discharging current of the sub-module capacitor of the MMC is near 50 Hz. Whereas the current of the AC system feeding into the fault point through the MMC corresponds to $f_o = 300$ Hz.

C. WT Algorithm

The high-frequency components of fault currents decay rapidly in the time domain. The WT algorithm has a good time-domain resolution in the high-frequency band of the signal and is ideally suitable for the analysis of extracting these fast-varying high-frequency components [22]-[24]. Equation (4) is the continuous WT (CWT) of the calculated signal $f(t)$.

$$C_{WT}(a,b) = \int_{-\infty}^{\infty} f(t)\frac{1}{\sqrt{a}}\psi\left(\frac{t-b}{a}\right)dt \qquad (4)$$

where $\psi(\cdot)$ is the mother wavelet function; a is the scale factor; and b is the translation factor.

In engineering practice, all the signals are discrete, which can be extracted by discrete WT (DWT). For a discrete signal sample $a_o(k)$, the smoothing approximation coefficient $a_j(k)$ and detail coefficient $d_j(k)$ of the jth layer are shown in (5).

$$\begin{cases} a_j(k) = \sum_n a_{j-1}(n)h_0(n-2k) \\ d_j(k) = \sum_n a_{j-1}(n)h_1(n-2k) \end{cases} \qquad (5)$$

where h_0 and h_1 are the low-pass filter and high-pass filter, respectively.

In this paper, the DbN-DWT is selected to extract the frequency components of the fault current. The higher the order

N, the smaller the high-frequency coefficient of the signal, and the more concentrated the signal energy. Meanwhile, the smaller the order N, the rougher the frequency band division, and the more dispersed the energy. Combining the effectiveness and computational efficiency, the DbN-DWT is adopted and a 4-layer decomposition is performed to extract feature quantities of the fault signal, as shown in Fig. 3, where f_0 is the signal frequency.
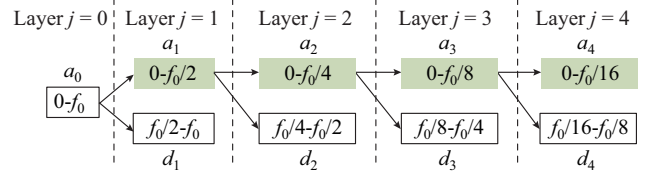

Fig. 3. Feature quantities of fault signal extracted by DdN-DWT.

III. RESTORATION STRATEGY FOR P-P FAULT

For a multi-source network with multiple MMCs, during the fault restoration process, the faulty line will be fed by the MMC at both ends of the line. The current of the MMC fed to the faulty point will be superimposed. Meanwhile, the mutual influence between the MMCs will be increased, which poses a challenge to the fault restoration strategy based on single-ended quantities. The proposed fault restoration strategy mainly includes the split method and faulty branch line identification method based on the transient energy of fault current.

A split method is proposed, which splits the double-ended power supply network into two mutually independent single-ended power supply networks, as shown in Fig. 4 and Fig. 5, where $R_{Rx} = R_{line}x/L_{14}$, $L_{14} = x + y$ is the length of the line L_{14} between MMC1 and MMC2; $L_{Rx} = L_{line}x/L_{14}$; $R_{Ry} = R_{line}y/L_{14}$; $L_{Ry} = L_{line}y/L_{14}$; and I_x, I_y, U_x, and U_y are the fault currents and voltages in both fault loops. After splitting, the superimposed influence of multiple MMCs on the branch can be effectively avoided.

Fig. 4. Two independent single-ended power supply networks under an NPF situation when L_{14} is split. (a) Single-ended power supply network at MMC1 side. (b) Single-ended power supply network at MMC2 side.

A. Procedure of Split Method for Double-ended Power Supply Network

The split method proposed in this subsection needs to be used in conjunction with reclosing. By closing the HDCCBs at both sides of the line according to a certain sequence, the fault information can be collected to determine the faulty branch line.
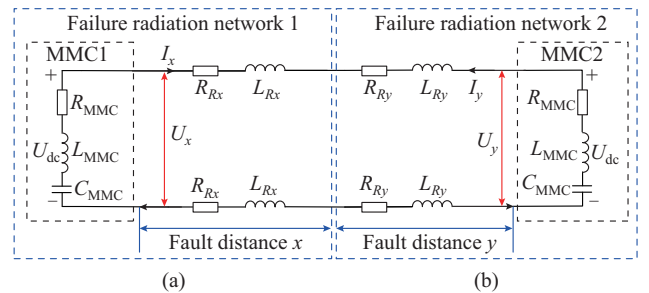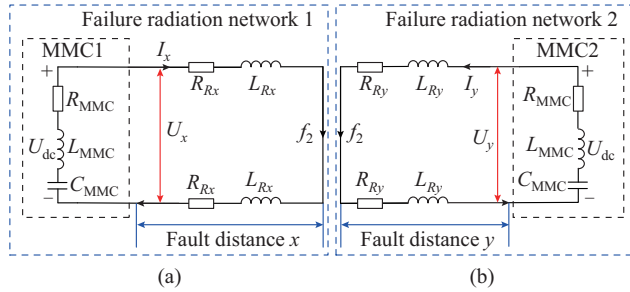
Fig. 5. Two independent single-ended power supply networks under a PF situation when L_{14} is split. (a) Single-ended power supply network at MMC1 side. (b) Single-ended power supply network at MMC2 side.

According to the above analysis, the reclosing process can be divided into the following two steps.

1) Close the HDCCB in area A1 at the MMC1 side. Subsequently, MMC1 will feed current into the line, while HDCCB in area B4 at the MMC2 side is still in the open state. If the fault property is NPF, it means that there is no fault point on the line before HDCCB in area A1 is closed. The MMC1 side has completed the reclosing operation, as shown in Fig. 4(a).

2) After a certain fixed time delay, close the HDCCB in area B4 at the MMC1 side. The MMC2 side will also complete the reclosing operation. Thus, both MMC1 and MMC2 will supply the power normally, and the system will return to its normal state, as shown in Fig. 4(b).

If the fault property is PF, the fault still exists before the HDCCB in area A1 is closed. The fault point and the MMC1 are in the same fault circuit, as shown in Fig. 5(a). Thus, the current flowing into the fault point from MMC1 continues to increase. The faulty line protection device in area A1, A2, A3, or A4 which is close to the MMC1 side needs to be selected and activated quickly so that the MMC1 side can be disconnected from the fault point. Following the same logic, after a certain fixed time delay, the HDCCB in area B4 is closed. And the fault point and the MMC2 converter are in the same fault circuit, as shown in Fig. 5(b). The faulty line protection device in area B1, B2, B3, or B4 which is close to the MMC2 side also needs to be tripped.

The procedure of the split method is as follows, and the logic sequence diagram is shown in Fig. 6.
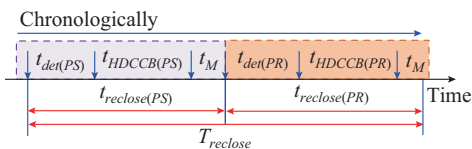

Fig. 6. Logic sequence diagram of fault restart split method.

1) *Step 1*: close the HDCCB of the power sending end, and judge the fault property (PF or NPF). For the PF, the corresponding HDCCB needs to be actuated, while for the NPF, the MMC1 side completes a fault restoration.

2) *Step 2*: perform the same operation on the power receiving end.

In Fig. 6, the subscript *det* represents the single-ended de-

tection time of the split method, and the following goals are mainly accomplished through the detection: determine whether the fault property is PF or NPF; and identify the faulty line. The subscript *HDCCB* represents the HDCCB action time, which is selected as 2 ms in this paper. The subscripts *PS* and *PR* represent the power transmitting end and the power receiving end, respectively. The subscript *M* represents the margin; and $t_{reclose}$ is the reclose time of the MMC at one side.

B. Procedure of Identification Method for Fault Branch Line

When a PF occurs on line L_{14}, the influence of the transition resistance is not considered. During the fault restoration period, when the HDCCB in area A1 at the MMC1 side is closed, the fault current will only be affected by the impedance value of the fault loop, which is positively correlated with the distance to the fault. The fault current provided by the single-ended power supply network varies with the distance from the MMC1 to the fault point, as shown in Fig. 7, where I_{setA1}, I_{setA2}, I_{setA3}, and I_{setA4} are the fault currents corresponding to the faults at the end of L_{141}, L_{142}, L_{143}, and L_{144}, respectively.
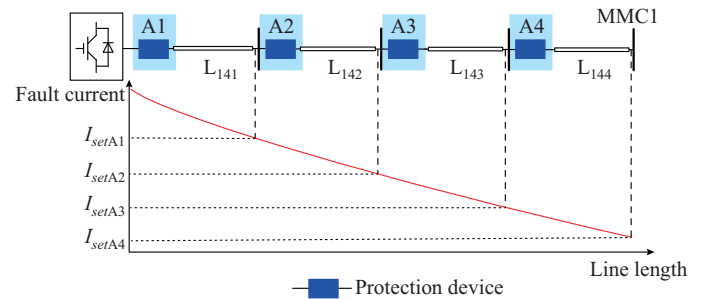

Fig. 7. Schematic diagram of fault current provided by single-ended power supply network at MMC1 side.

In the NPF case, the current characteristics are more obvious and the characteristics of the current energy are considered to distinguish the faulty branch line. Use DbN-DWT to extract the low-frequency information of the fault current. And the sum of squares of wavelet coefficients is used to characterize the transient energy of fault current in a fixed frequency band time window.

Take the PF at point f_2 in L_{142} as an example. The HDCCB in areas A1 and B4 will receive a trip command to remove the entire line of L_{14} after a fault occurs. At this point, the fault restoration phase is activated and the HDCCB in area A1 at the MMC1 side needs to be closed as the first step of fault restoration. The fault current is fed from MMC1 to f_2 through areas A1 and A2. Using the transient energy of the fault current as that of the characteristic quantity, L_{142} is quickly identified as a faulty line. Subsequently, the HDCCB in area A2 will complete the tripping behaviour immediately, isolate the MMC1 and f_2 perfectly, and prevent the formation of electrical circuits. Since the HDCCB in area A2 is in the open state, MMC1 does not feed f_2, as shown in Fig. 8(a).

Following the same logic, the second step of the fault restoration is started. The HDCCB in area B4 at the MMC2

side completes the closing operation. The fault current in the fault circuit is fed from MMC2 to f_2 through areas B4, B3, and B2. Using the same judgment method, L_{142} is judged to be a faulty branch line, and the DCCB in the B2 area acts, as shown in Fig. 8(b).
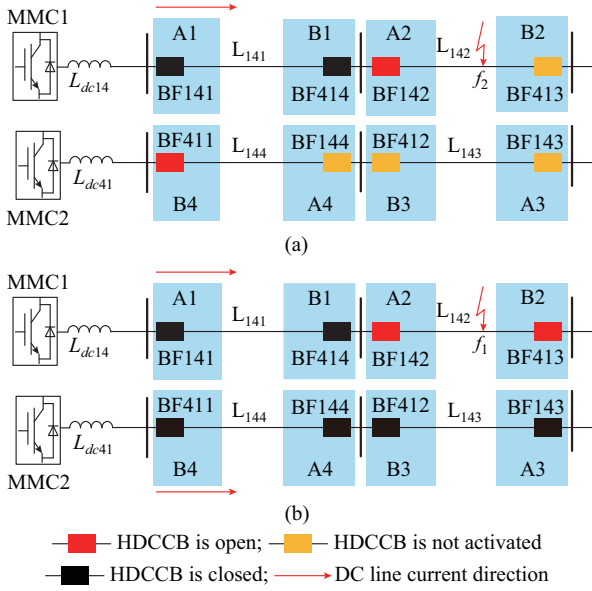

Fig. 8.   Description of fault restoration using proposed restoration strategy. (a) First step of fault restoration. (b) Second step of fault restoration.

Under the influence of noise and other special conditions, the transient energy of fault current calculated for the end of the line L_{141} and the first section of L_{142} may overlap. The overlapping part belongs to the unreliable area of the identification result, which may cause the HDCCB on the non-faulty line to malfunction, as shown in Fig. 9. The unreliable area can be reduced by selecting an appropriate threshold to cover the area. Within the reliable area, the transient energy of fault current can accurately identify and judge internal faults and external faults.
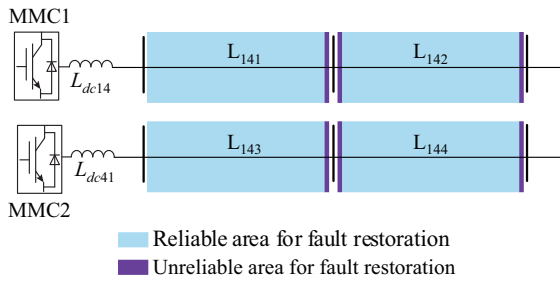

Fig. 9.   Diagram of trusted area of fault restoration strategy.

IV. COMPLETE SCHEME OF PROPOSED FAULT RESTORATION STRATEGY

Three functions must be met in the proposed strategy: ① the fault property can be distinguished, and the power supply can be restored smoothly under NPF; ② the type of fault can be identified, and only the faulty branch line for P-P faults is judged; ③ in the case of a PF fault, the faulty branch line can be determined, and a trip command can be

sent to the corresponding HDCCB to remove the fault again. As the strategy focuses on P-P faults, a fault type screening criterion is added within this section.

A. Distinguishing PF and NPF

According to Section III, when the HDCCB in area A1 at the MMC1 side is closed, regardless of whether the fault exists, MMC1 and MMC2 are isolated and cannot pass current. Therefore, the voltage information is used in this subsection to determine the fault property. For the NPF, the fault disappears before entering the fault restoration, while in the PF, the clamping voltage of the fault point is still affected after the fault restoration.

Take the PF at point f_2 of L_{142} as an example. When entering the first step of the fault restoration, the HDCCB in area A1 is closed, and the existence of point f_2 limits the voltage rise of the circuit. On the contrary, when an NPF fault occurs on L_{142}, fault point f_2 does not exist. The voltage of the circuit increases to the rated voltage with the closing of HDCCB in area A1. Similar characteristics also exist in the second step of fault restoration. In summary, the characteristic of voltage rise degree is used to distinguish PF and NPF.

In this subsection, $0.85U_{bus}$ is chosen as the rectification value, and U_{bus} is the normal operating bus voltage. A single voltage data point cannot reliably distinguish PF and NPF. Therefore, the 3 ms data window is chosen for the simulation process.

The reclosing criterion can be expressed as:

$$\sum_{i=1}^{N_{re}} \left| U_i \right| > N_{re} k_{reclose} |U_{bus}| \qquad (6)$$

where $k_{reclose}$ is the reliability coefficient, which is selected as 0.85 [18]; N_{re} is the number of the data points of the 3 ms data window, which is 3×20; and U_i is the collected line voltage. It is stipulated that if the criterion of (6) is satisfied, the NPF occurs on the line, which is recorded as S1=0. Otherwise, the PF occurs on the line, which is recorded as S1=1.

B. Distinguishing P-G and P-P Faults

The proposed strategy is mainly applicable to P-P faults, so further identification of the fault type is required. For a P-P fault at point f_2 on L_{142}, the positive and negative lines constitute a faulty circuit. The positive and negative currents are equal and much larger than the steady-state current. However, when a P-G fault occurs at point f_2 on L_{142}, the current of the fault pole increases rapidly and is much larger than the steady-state current. Though the current of the non-fault pole will be affected by the fault pole, it will remain the value near the steady-state current. Therefore, the relationship between the positive current and the negative current can be used to accurately distinguish the fault type.

Assume that the positive and negative currents are x_1 and x_2, respectively, which are shown in (7). The calculation method of the Pearson correlation coefficient ρ of x_1 and x_2 is shown in (8). When the criterion of (9) is satisfied, a P-P fault occurs in the line. While when the criterion (10) is satisfied, a P-G positive line fault occurs; otherwise, a P-G negative line fault occurs.

$$\begin{cases} |x_1| = \dfrac{1}{N_{re}} \sum_{i=1}^{N_{re}} x_{1i} \\[4mm] |x_2| = \dfrac{1}{N_{re}} \sum_{i=1}^{N_{re}} x_{2i} \end{cases} \tag{7}$$

$$\rho(x,y) = \frac{\displaystyle\sum_{i=1}^{N_{re}} (x_{1i} - \bar{x}_1)(x_{2i} - \bar{x}_2)}{\sqrt{\displaystyle\sum_{i=1}^{N_{re}} (x_{1i} - \bar{x}_1)^2}\ \sqrt{\displaystyle\sum_{i=1}^{N_{re}} (x_{2i} - \bar{x}_2)^2}} \tag{8}$$

$$\rho(x,y) > \rho_{set} \tag{9}$$

$$\begin{cases} |x_1| > |x_2| \\ \rho(x,y) < \rho_{set} \end{cases} \tag{10}$$

where x_{1i} and x_{2i} are the instantaneous values of the positive and negative currents collected, respectively; $\bar{x}_1$ and $\bar{x}_2$ are the average values of the positive and negative currents collected, respectively; and ρ_{set} is the setting value, which is selected as 0.9.

For P-P faults, the positive and negative currents are the same, and the ideally calculated Pearson correlation coefficient is always 1. However, for a P-G positive line fault, the positive pole current continues to increase, and its current value x_1 is greater than 0; while the negative pole current value x_2 fluctuates up and down around 0. Since $|x_1| > |x_2|$, the Pearson correlation coefficient is less than 1.

The theoretical interval of the Pearson correlation coefficient in statistics is $[-1, 1]$. When a P-P fault occurs on the line, the Pearson correlation coefficient is approximately 1. Considering the Harsh working conditions such as noise, a margin region is set to improve the reliability of the judgment result, as shown in Fig. 10. The threshold value is 10%, which means that the setting value ρ_{set} is determined to be 0.9.

If the coefficient $\rho \in [0.9, 1]$, it is considered as a P-P fault, and it is recorded as S2 = 1. However, if the coefficient ρ is not in that range and $|x_1| > |x_2|$, it is considered as a P-G positive line fault; otherwise, it is considered as a P-G negative line fault. Whether there is a P-G positive or P-G negative line fault, it is recorded as S2 = 0.
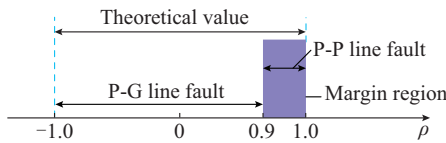

Fig. 10.   Margin region of Pearson correlation coefficient.

C. Distinguishing Faulty Branch Line Under PF

According to the analysis in Section III, in a single-ended power supply network, its fault current can be approximately equated to a smooth curve only related to the fault distance, as shown in Fig. 7. The fault current is mainly concentrated in the low-frequency section. Compared with the instantaneous current value, the transient energy of fault current calculated by the wavelet low-frequency coefficient can better characterize the fault. Thus, this section uses the transient en-

ergy of fault current to construct a faulty branch line identification scheme without delayed action.

The calculation method of the transient energy of fault current in a fixed frequency band is as follows: select DbN-DWT to obtain the scale coefficient, and calculate the sum of squares of the scale coefficient in the time window of 5 ms. It can be expressed as:

$$E_i = \sum_{k=N_1 + f\Delta T_{i-1}}^{N_1 + f\Delta T_i} L_{able} A_k^2 \tag{11}$$

where E_i is the transient energy of fault current of the ith data; f is the sampling frequency, which is chosen as 20 kHz in this paper; N_1 is the sampling point where the fault occurs; ΔT_i is the time window of 5 ms of the ith data; A_k is the frequency coefficient under the 2^k scale of the WT; and L_{able} is the value representing the positive and negative directions of the current, and when the current is in the positive direction, $L_{able} = 1$, otherwise, $L_{able} = 0$. The incoming line from the MMC side is assumed to be the positive direction in this paper.

Take the HDCCB in area A1 at the MMC1 side as an example. Assume that E_{setA1}, E_{setA2}, E_{setA3}, and E_{setA4} are the setting values of A1, A2, A3, and A4, respectively, which are the transient energies of fault current corresponding to the fault at the end of the line. There is a step difference in the current of each branch line, and the transient energy of fault current will further amplify this difference characteristic. Thus, the setting values of A1, A2, A3, and A4 have a certain degree of selectivity. And the action setting value is the setting value multiplied by a reliability factor.

When the fault occurs in the areas of L_{141}, L_{142}, L_{143}, and L_{144}, the corresponding fault transient energy is recorded as E_{A1}, E_{A2}, E_{A3}, and E_{A4}. Then, it is compared with the action setting value of each branch line. If it is greater than the action setting value, it is judged as a faulty branch, and a trip command is issued to the HDCCB of the line. Afterwards, the HDCCB in area B4 at the MMC2 side is closed immediately. If E_{A1} is greater than $k_{set} E_{setA1}$, L_{141} is considered to be a faulty branch line, and HDCCB in the A1 area will trip. The corresponding criterion can be expressed as:

$$E_{Ai} > k_{set} E_{setAi} \quad i = 1, 2, 3, 4 \tag{12}$$

Under PF faults, the fault current curve is considered a continuous one. The corresponding transient energy curve of the fault current can also be regarded as a continuous one. To ensure the maximum protection range, the value of the reliability coefficient can be reduced. In the most ideal case, k_{set} can be set to be 1.

Following the same logic, E_{setB1}, E_{setB2}, E_{setB3}, and E_{setB4} are assumed to be the setting values of B1, B2, B3, and B4, respectively. The corresponding criterion can be expressed as:

$$E_{Bi} > k_{set} E_{setBi} \quad i = 1, 2, 3, 4 \tag{13}$$

If the criteria of (12) and (13) are met, the corresponding Ai (i = 1, 2, 3, 4) and Bi (i = 1, 2, 3, 4) belong to an internal PF. The corresponding HDCCB needs to be tripped, which is recorded as SAi = 1 and SBi = 1. If the criteria are not met, an external PF occurs on the corresponding branch line, which is recorded as SAi = 0 and SBi = 0.

There is a time interval between the HDCCBs in areas A1

and B4. The length of the time interval depends on the fault detection, HDCCB action, and DC arc extinction, as shown in Fig. 11. From the fault restoration which is treated as the starting point, a data window of 3 ms (denoted by Δt_{S1}) is selected backwards to judge the fault property (PF or NPF) and the fault type (P-P or P-G). Meanwhile, a data window of 5 ms (denoted by Δt_{S2}) is selected backwards to judge the faulty branch line, and the HDCCB trip time is 2 ms. Finally, a data window of 8 ms is selected as the arc extinction time.
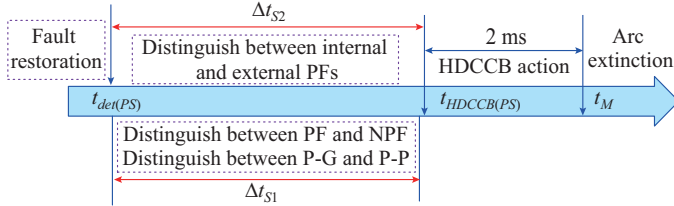

Fig. 11.   Timing coordination diagram of fault restoration.

Based on the above analysis, a logical block diagram of the proposed strategy is shown in Fig. 12. The logic diagram of the HDCCB signal in the corresponding area under the internal PF condition is shown in Fig. 13.
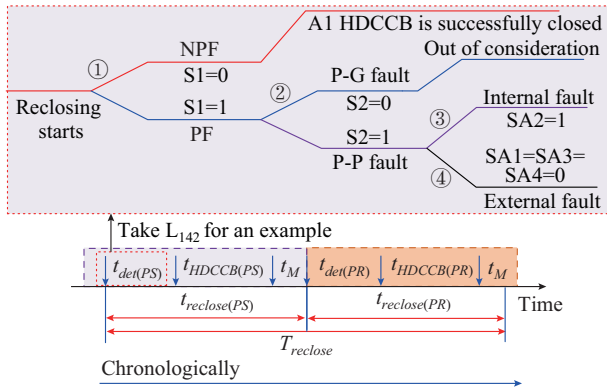

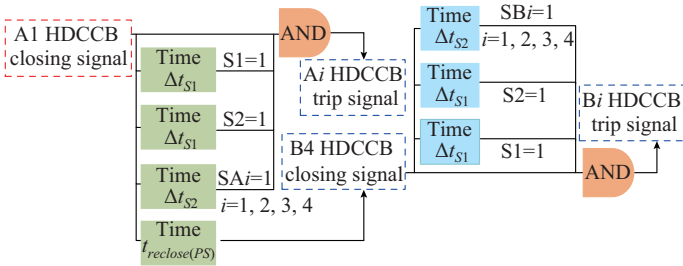Fig. 12.   Logic diagram of proposed strategy.

Fig. 13.   Logic diagram of HDCCB signal in corresponding area under PF condition.

It can be observed from Fig. 12 that the complete fault restoration is composed of two parts, i.e., the PS and PR restorations. Each part can be divided into three steps according to the chronological order: ① judge the PF (S1=1); ② judge the P-P fault (S2=1); ③ judge the faulty branch line area (SAi=1 and SBi=1). According to the given logic, the PS is first judged, and then the PR is judged. The PS and PR restorations are independent of each other, and only have a time difference between their actions. The logic of the signal adopts "AND" gates. When the three steps are satisfied,

the corresponding HDCCB completes the tripping process. It can effectively reduce the error rate and the action rate of the HDCCB. Based on the results of the various criteria mentioned in Fig. 12, Fig. 13 shows the union relationship between the results. Only when the three judgment results are all 1, the HDCCB trip command will be generated. Finally, a flowchart of the fault restoration strategy based on the transient energy of fault current is shown in Fig. 14.
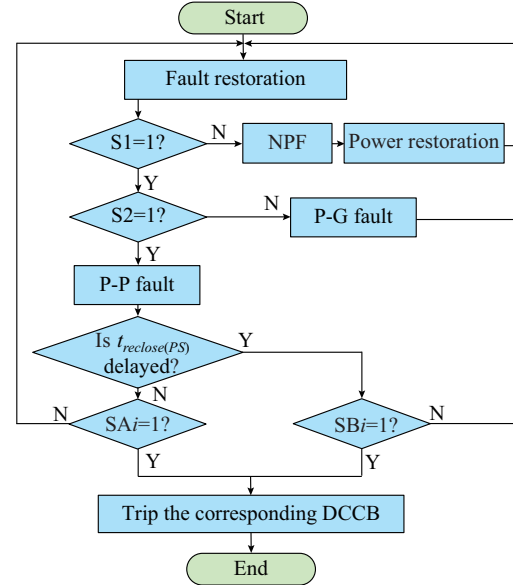

Fig. 14.   Flowchart of fault restoration strategy based on transient energy of fault current.

V. SIMULATION TESTS

A multi-terminal flexible DC distribution network with MBLs described in [10] is simulated based on the PSCAD/EMTDC, whose topology and parameters are shown in Fig. 15 and Tables I and II. The DC distribution network is composed of four lines L_{14}, L_{15}, L_{16}, and L_{17}, and each line is composed of four branch lines with the same length. Take L_{14} for example, $L_{14}=L_{141}+L_{142}+L_{143}+L_{144}$. The model studied in this paper is extensible, and the number of MMC terminals and branch lines can be freely combined. A P-P fault at f_2 on the branch line L_{142} is supposed to verify the feasibility of the proposed strategy. Assume that the fault point f_2 is 10 km away from the first section of L_{142}, and the first section of L_{142} is close to MMCB2.

A. Judgment Result of PF and NPF

In the fault restoration phase, the HDCCB in the area A1 at the MMCB2 side will be closed first. For NPFs, the line voltage will quickly increase to $0.85U_{bus}$ and then stabilize to U_{bus}. However, for PFs, the line voltage will be limited to very low levels, approximately zero, due to the presence of the fault point.

The time window chosen for this subsection is 3 ms, so the basic setting value is chosen to be 51. In the case of an NPF, the climbing degree of the line voltage is greater than 51, while in the case of a PF, the climbing degree of the line voltage is less than 51. Figure 16 shows the judgment results between the PF and NPF, and the results are correct.
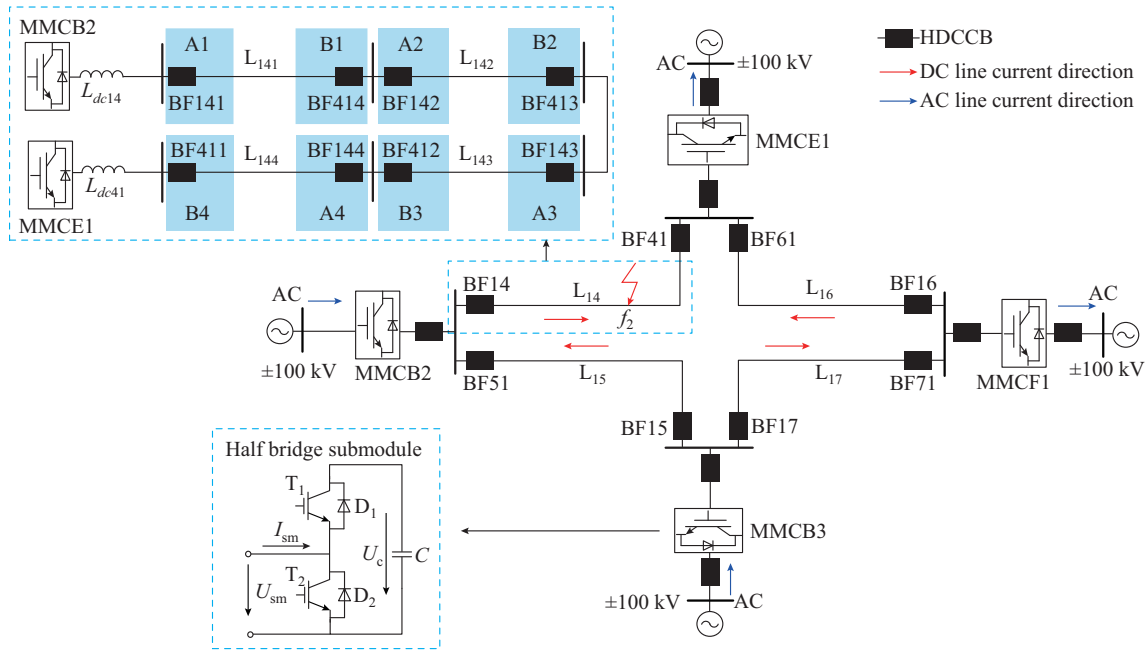
Fig. 15.   Schematic diagram of a multi-terminal flexible DC distribution network with MBLs.

TABLE I
PARAMETERS OF MULTI-TERMINAL FLEXIBLE DC DISTRIBUTION NETWORK

Unit	Capacity (MW)	Inductance of bridge arm (mH)	Sub-module voltage (kV)	Line inductance (mH)	Control model	Starting time (s)
MMCB2	80	20	2.6	50	Power	0.4
MMCB3	120	20	2.6	50	Power	0.4
MMCE1	−120	20	2.6	50	Power	0.4
MMCF1	−80	20	2.6	50	Voltage	0.2

TABLE II
DC LINE PARAMETERS OF MULTI-TERMINAL FLEXIBLE DC DISTRIBUTION NETWORK

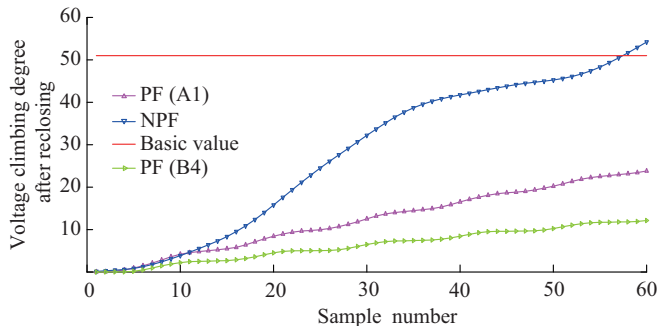| Line	Length (km)	Line	Length (km)
L_{14}	100	L_{16}	100
L_{15}	100	L_{17}	100
L_{141}	25	L_{143}	25
L_{142}	25	L_{144}	25

Fig. 16.   Judgment result of PF and NPF.

B. Judgment Result of P-P and P-P Faults

As mentioned above, after a P-P occurs, the positive and negative currents are in the same fault circuit, and the calculated Pearson correlation coefficient is always 1. However, the change trends of the positive and negative currents are different, and the corresponding Pearson correlation coefficient is less than 1. Meanwhile, the longer the data window, the greater the difference between the Pearson correlation coefficients corresponding to P-P and P-G faults. The Pearson correlation coefficient can correctly distinguish P-P and P-G faults, and the results are shown in Fig. 17.
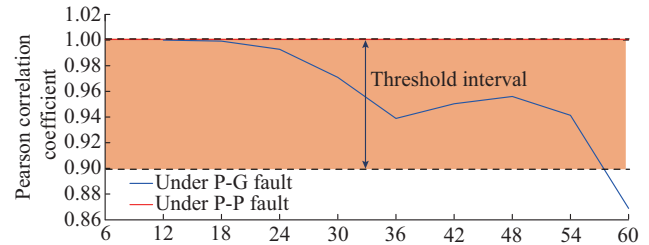

Fig. 17.   Judgment results of P-P and P-G faults.

If the judgment result is a P-P fault, the proposed strategy needs to be used to identify the faulty branch line.

C. Judgment Results of Faulty Branch Line Under PF

Take L_{14} as an example. By performing the fault simulation at different locations in the line L_{14}, the action setting values ($k_{set}E_{setA1}$, $k_{set}E_{setA2}$, $k_{set}E_{setA3}$, $k_{set}E_{setA4}$, $k_{set}E_{setB1}$, $k_{set}E_{setB2}$, $k_{set}E_{setB3}$, and $k_{set}E_{setB4}$) corresponding to L_{141}, L_{142}, L_{143}, and L_{144} after a P-P Fault are calculated and shown in Table III.

In the fault restoration phase, the HDCCB in area A1 at the MMCB2 side will be closed first. E_{A1}, E_{A2}, E_{A3}, and E_{A4} are calculated according to (11), respectively, and are compared with the setting values in Table III. Among them, the

area A2 satisfies (12), thus an internal PF occurs on the line L_{142}. The lines L_{141}, L_{143}, and L_{144} belong to the external PF area, and the judgment results are shown in Fig. 18(a).

TABLE III
ACTION SETTING VALUES CORRESPONDING TO EACH BRANCH LINE AFTER P-P FAULT

Parameter	Value	Parameter	Value
$k_{set}E_{setA1}$	8820.7074	$k_{set}E_{setB1}$	2732.1038
$k_{set}E_{setA2}$	5717.2154	$k_{set}E_{setB2}$	3726.5430
$k_{set}E_{setA3}$	3982.9371	$k_{set}E_{setB3}$	5264.1395
$k_{set}E_{setA4}$	2939.3843	$k_{set}E_{setB4}$	8039.1475

After a fixed time delay, the HDCCB in area B4 at the MMC2 side starts to be closed. E_{B1}, E_{B2}, E_{B3}, and E_{B4} are calculated according to (11), and are compared with the setting values in Table III. Among them, area B2 satisfies (12), and it is also judged that L_{142} belongs to the internal PF area, as shown in Fig. 18(b).
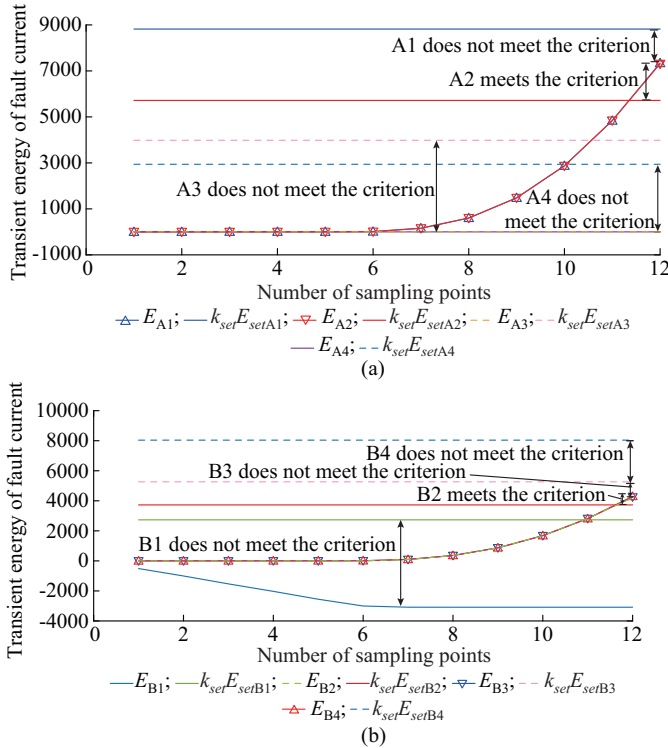

Fig. 18. Judgment results of faulty branch line during fault restoration. (a) Judgment results of area A1 at MMCB2 side after reclosing. (b) Judgment results of area B4 at MMCE1 side after reclosing.

Further, the P-P faults are tested for different fault locations, and the identification results are shown in Tables IV and V. The extensive PSCAD simulation test results show that the proposed strategy is feasible. During the fault restoration process, the NPF disappears, the HDCCB in the corresponding area is successfully closed, and the system can quickly restore power. For PFs, the faulty branch line can be accurately identified through the transient energy of fault current. After receiving the trip command, the HDCCB quickly clears the faulty branch line, and effectively reduce the risk of the system.

TABLE IV
IDENTIFICATION RESULTS OF NPFS AND PFS FOR P-P FAULTS

Fault location (km)	Voltage rise degree	Result	Fault location (km)	Voltage climbing degree	Result
0 (L_{141})	0.1482 / 33.1373	PF	25 (L_{142})	23.8216 / 22.8485	PF
0 (L_{142})	15.2294 / 29.6272	PF	0 (L_{143})	23.8442 / 22.7465	PF
5 (L_{142})	17.1269 / 28.0391	PF	25 (L_{141})	55.0230 / 61.2443	NPF
10 (L_{142})	18.6889 / 26.2827	PF	25 (L_{142})	55.2644 / 61.3287	NPF
15 (L_{142})	20.8027 / 25.8373	PF	25 (L_{143})	55.0471 / 61.2848	NPF
20 (L_{142})	22.6822 / 24.7648	PF	25 (L_{144})	55.0536 / 61.3147	NPF

Note: 0 (L_{141}) represents that the fault occurs on the L_{141}, and the number 0 represents the length from the fault point to the first section of L_{141}.

TABLE V
RESULTS OF FAULTY BRANCH LINE UNDER DIFFERENT FAULT LOCATIONS

Fault location (km)	E_{A1}	E_{A2}	E_{A3}	E_{A4}	E_{B1}
0 (L_{142})	8806.3078	8842.0090	0.0002	0.0002	−3590.0726
5 (L_{142})	8025.3962	7988.2350	0.0008	0.0008	−4001.9702
10 (L_{142})	7340.1826	7309.7326	0.0005	0.0005	−3085.1784
15 (L_{142})	6734.5854	6734.5854	0.0002	0.0002	−3677.2409
20 (L_{142})	6193.8273	6186.5776	0.0001	0.0001	−3301.2361
25 (L_{142})	5731.1939	5717.2154	0.0017	0.0017	−4110.3430

Fault location (km)	E_{B2}	E_{B3}	E_{B4}	Result
0 (L_{142})	3726.5430	3753.1245	3753.6617	A2 and B2 action
5 (L_{142})	4039.1613	4012.1543	3965.9890	A2 and B2 action
10 (L_{142})	4199.7794	4251.1549	4296.2598	A2 and B2 action
15 (L_{142})	4591.1283	4590.1941	4548.7494	A2 and B2 action
20 (L_{142})	4849.4298	4894.1604	4934.4430	A2 and B2 action
25 (L_{142})	5238.0929	5275.4891	5315.0862	A2 and B2 action

Ideally, the full length of the line can be identified according to the principle of the action setting values. For a 25 km line, when the length of the faulty line is 20 km, the ratio of the calculated value of the transient energy of fault current to the setting value is greater than 1.08. This means that the protection range of the line in 80% of the area has a certain selectivity. Therefore, the transient energy of fault current can effectively identify internal and external PFs. The adaptability and robustness of the proposed strategy for different situations are further considered.

D. Influence of Noise

Anti-noise analysis is carried out on the identification results of internal and external PFs, and the noise is Gaussian white noise. The signal-to-noise ratios of 10, 20, 30, 40, 50 dB, and infinity (no noise) are selected as variables, respec-

tively. No matter what the signal-to-noise ratio is, the transient energy of fault current does not fluctuate greatly during the fault restoration process. Even if the signal-to-noise ratio is 10 dB, the faulty branch line L_{142} can still be correctly identified, as shown in Fig. 19.
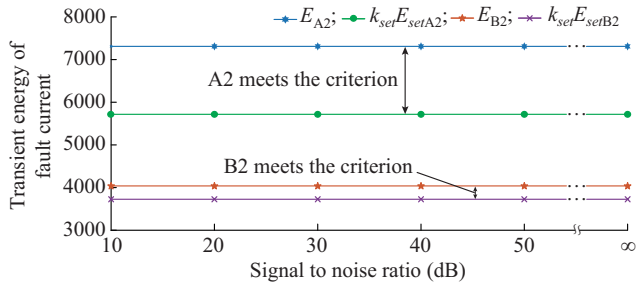

Fig. 19. Identification results of faulty branch line under different signal-to-noise ratios.

The Gaussian white noise is essentially random data with the mean value of zero and non-zero variance. The mean value of zero will not affect the calculation results of (11). With a noise level of 10 dB, the results are all correct. Therefore, the proposed strategy has a strong anti-noise ability.

E. Influence of DC Arc Equivalent Resistance

According to (12), L_{142} is judged to be a faulty branch line, the corresponding HDCCB in area A2 will receive a trip instruction. During the fault restoration process, the amplitude of the fault current corresponding to different conditions is different, and the time required to extinguish the DC arc after the HDCCB action is also different. Ideally, before the HDCCB in area B4 at the MMCE1 side is closed, the arc in area A2 is completely dissipated. However, in most cases, there is still a small amount of DC arc in area A2, which will affect the identification results of the faulty lines during the restoration process of the HDCCB in area B4 at the MMCE1 side.

In PSCAD, the nature of the opening state of HDCCB is equivalent to connecting a large resistor (1 MΩ) in series in the system. The DC arc is simulated by adjusting the value of the series resistance. Further, the identification results of fault areas are analyzed when the equivalent resistance of HDCCBs is different. According to the static characteristics of the arc of the improved Mayr model, when the current is less than 0.5 kA, the arc equivalent resistance will be greater than 12 Ω.

Take a P-P fault at L_{143} as an example. The smaller the equivalent resistance of the HDCCB, the larger the corresponding DC arc. When the DC arc is too large, it is easy to cause the fault to recur. In this paper, after $t_{reclose(PR)}$, the feed-in current to the fault point at the MMCB2 side is less than 0.5 kA, so the minimum equivalent resistance of the arc is considered to be 12 Ω.

In this subsection, the DC equivalent resistance is replaced by a constant resistance, and the minimum equivalent DC arc resistance of the HDCCB is 10 Ω. According to the identification results in Fig. 20, the L_{141}, L_{142}, and L_{144} in areas B1, B2, and B4 are identified as the external PFs, and

the L_{143} in the area B3 is identified as the internal PF. The correct identification results demonstrate that under the reasonable equivalent resistance of DC arc, the performance of the proposed strategy will not be affected.
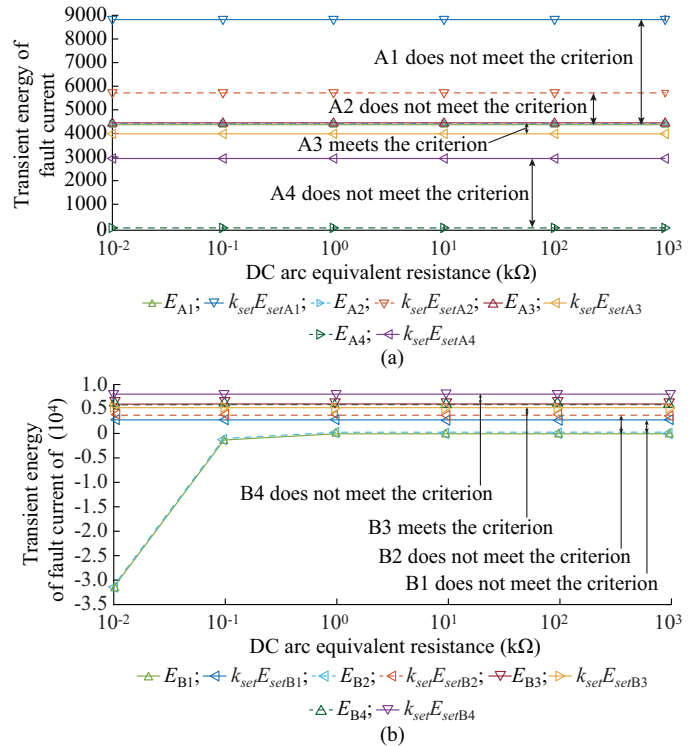

(a)

(b)

Fig. 20. Identification results of fault areas under different DC arc equivalent resistance. (a) Identification results of fault areas A1, A2, A3, and A4. (b) Identification results of fault areas B1, B2, B3, and B4.

Taking area B1 as an example, the two main influencing factors, i.e., the fault location and the DC arc equivalent resistance, are considered simultaneously. The identification results of the area B1 under different DC arc equivalent resistances and fault locations are shown in Fig. 21. The value of E_{B1} changes greatly with the change of DC arc equivalent resistance. When the DC arc equivalent resistance is 10 Ω or higher, E_{B1} does not satisfy the criterion of (13), and the corresponding HDCCB in the area B1 does not operate, which demonstrates that the proposed strategy has good adaptability.
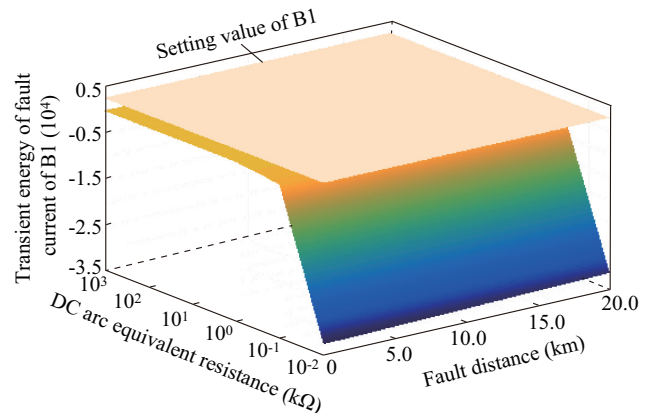

Fig. 21. Identification results of area B1 under different DC arc equivalent resistances and fault locations.

F. Influence of Number of Sub-modules in MMC

Assume that other parameters do not change, and only the number of sub-modules in the MMC is changed. The number varies from 38 to 200 and the identification results of the fault areas are shown in Fig. 22. The transient energy of fault current with the number of sub-modules of 50 is used as the threshold value. It can be observed that when the number of sub-modules is greater than or equal to 50, the identification results are correct and will not affect the identification results.
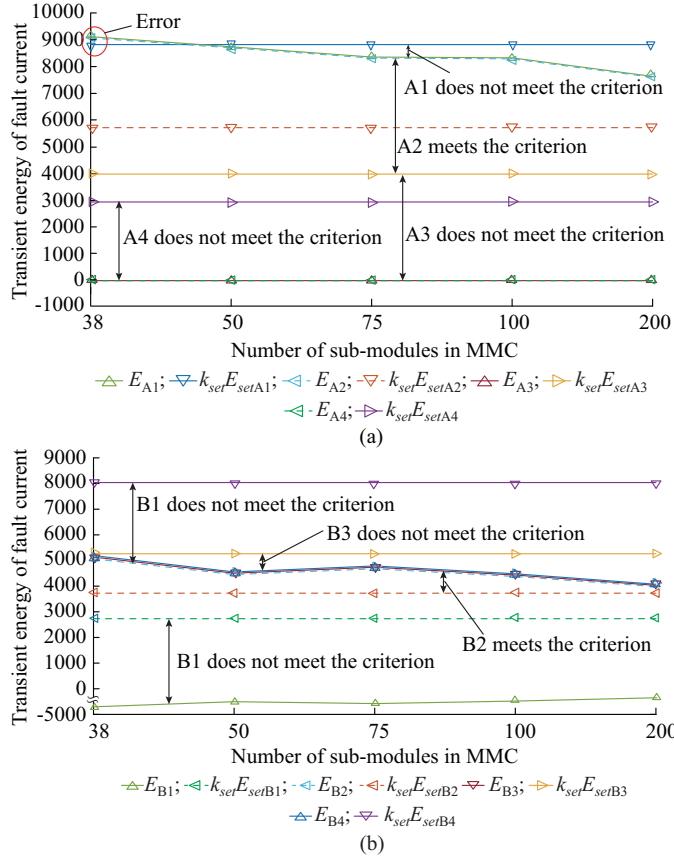

Fig. 22. Identification results of fault areas under different numbers of sub-modules in MMC. (a) Identification results of fault areas A1, A2, A3, and A4. (b) Identification results of fault areas B1, B2, B3, and B4.

When the number of sub-modules is 38, it can be observed that there is an error in the identification result at the PS side, and the calculation result is approximately equal to the threshold value. The decrease of the number of sub-mod-

ules increases the transient energy of fault current appropriately, but the increased value is limited. The results demonstrate that the proposed restoration strategy can meet the requirements, and the minimum number of sub-modules can be used as a parameter in the actual engineering calculation of the setting value.

G. Influence of Different Control Modes for MMCs

The network shown in Fig. 15 takes the occurrence of permanent P-P faults on branch line L_{142} as the research object.

Assuming that other parameters do not change, and only the control mode of MMCE1 is changed, the identification results of the fault areas are shown in Table VI. It can be recognized that L_{142} is a faulty branch line, and the HDCCB in areas A2 and B2 are opened in sequence. The change of MMCE1 control mode has little effect on the proposed fault restoration strategy.

H. Scalability Analysis of Proposed Fault Restoration

The proposed strategy focuses on models containing MBLs. This strategy only involves the coordination problem of MBLs between two MMCs. And the strategy is independent of the line type (overhead line or cable), the number of branch lines, and the number of MMCs. Therefore, the proposed strategy can be easily extended to various topology scenarios with MBLs and has good scalability.

I. Influence of Main Protection Malfunctions

Suppose a P-P fault occurs at line L_{16}, the main protection of line L_{14} malfunctions, and the areas A1 and B4 give a trip command to the corresponding HDCCBs. To analyze the applicability performance of the proposed strategy under this operating condition, three cases are set up according to the different entry reclosing times of lines L_{14} and L_{16}.

1) Case 1: L_{16} enters the fault restoration phase first, and after a fixed time delay, L_{14} enters the fault restoration phase.

2) Case 2: L_{16} and L_{14} enter the fault restoration phase at the same time.

3) Case 3: L_{14} enters the fault restoration phase first, and after a fixed time delay, L_{16} enters the fault restoration phase.

The fixed time delay chosen for this subsection is 2 ms.

The identification results of the fault area under different cases are shown in Fig. 23. For the situation that the main protection of line L_{14} is mis-activated and the normal line L_{14} is removed, since the line L_{14} does not have a fault point, the line L_{14} will be identified as an NPF during the fault restoration phase and will be put back into normal operation.

TABLE VI
IDENTIFICATION RESULTS WHEN CONTROL MODE CHANGES

Control mode	E_{A1}	E_{A2}	E_{A3}	E_{A4}	E_{B1}	E_{B2}	E_{B3}	E_{B4}	Result
MMCB2: CPC; MMCE1: CPC	7630.6648	7599.0315	0.000174200	0.0000537	−3186.41168	3983.0146	4032.4467	4074.7263	A2 and B2 operation
MMCB2: CPC; MMCE1: CVC	7685.2082	7653.4839	0.000071618	0.0000273	−3821.72448	4777.1556	4833.6714	4883.7324	A2 and B2 operation

VI. CONCLUSION

Generally, the probability of a non-permanent P-P fault in a flexible DC distribution system with MBLs is high. As the

traditional fault restoration strategy has its limitation in determining the faulty branch line, a novel fault restoration strategy is proposed to overcome such shortcomings for better distinguishing the faulty branch lines.
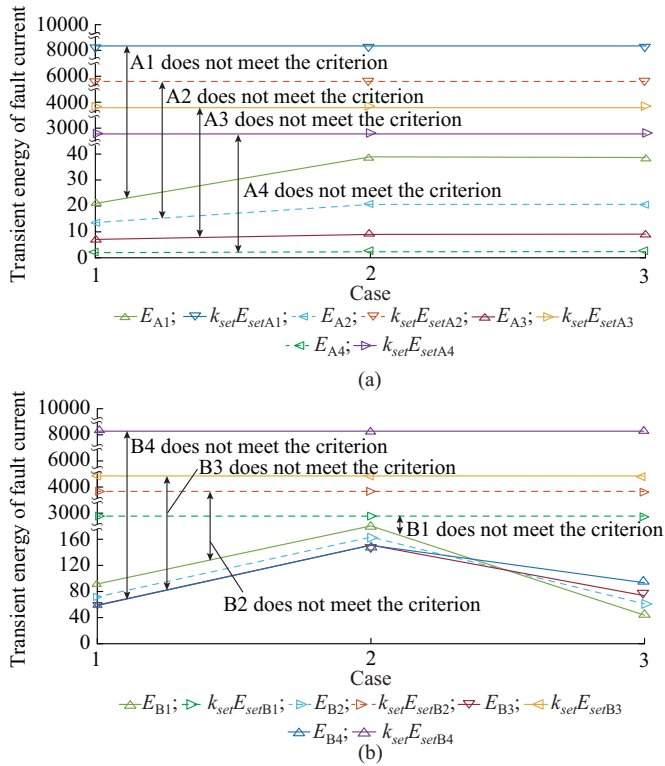
Fig. 23. Identification results of fault areas under different cases. (a) Identification results of fault areas A1, A2, A3, and A4. (b) Identification results of fault areas B1, B2, B3, and B4.

The proposed strategy cooperates with the reclosing strategy of the HDCCB. A split method is used to convert a double-ended supply network into two independent single-ended power supply networks. Then, a faulty line criterion is proposed based on the transient energy of fault current, which can be used to reliably identify faulty branch lines using only local information. Furthermore, the proposed strategy can also be used in conjunction with other fault restoration strategies.

It is worth pointing out that the proposed strategy still has some potential limitations: ① it cannot be applied to P-G fault in which the transition resistance is uncertain; ② it cannot be applied to the scenarios where the converter has multiple feeders; ③ it needs to further analyze and improve the unreliable area.

REFERENCES

[1] Y. Qi, S. Nicholas, J. He et al., "The policy-driven peak and reduction of China's carbon emissions," Advances in Climate Change Research, vol. 11, no. 2, pp. 65-71, Jun. 2020.
[2] L. Zheng, K. Jia, T. Bi et al., "Cosine similarity based line protection for large scale wind farms," IEEE Transactions on Industrial Electronics, vol. 68, no. 7, pp. 5990-5999, Jul. 2021.
[3] J. Duan, Z. Li, Y. Zhou et al., "Study on the voltage level sequence of future urban DC distribution network in China: a review," International Journal of Electrical Power & Energy Systems, vol. 117, p. 105640, May 2020.
[4] L. Zhang, J. Liang, W. Tang et al., "Converting AC distribution lines to DC to increase transfer capacities and DG penetration," IEEE Transactions on Smart Grid, vol. 10, no. 2, pp. 1477-1487, Mar. 2019.
[5] J. Wu, Z. Wang, L. Xue et al., "Key technologies of VSC-HVDC and its application on offshore wind farm in China," Renewable and Sustainable Energy Reviews, vol. 36, pp. 247-255, Aug. 2014.
[6] J. Li, Y. Li, L. Xiong et al., "DC fault analysis and transient average current based fault detection for radial MTDC system," IEEE Transactions on Power Delivery, vol. 35, no. 32, pp. 1310-1320, Jun. 2020.
[7] B. Li, Y. Li, and J. He, "A DC fault handling method of the MMC-based DC system," International Journal of Electrical Power & Energy Systems, vol. 93, pp. 39-50, Dec. 2017.
[8] B. Li, H. Gui, B. Li et al., "A permanent fault identification method for single-pole grounding fault of overhead transmission lines in VSC-HVDC grid based on fault line voltage," International Journal of Electrical Power & Energy Systems, vol. 117, p. 105603, May 2020.
[9] B. Li, J. He, Y. Li et al., "A novel DCCB reclosing strategy for the flexible HVDC grid," IEEE Transactions on Power Delivery, vol. 35, no. 1, pp. 244-257, Feb. 2020.
[10] B. Li, Q. Mao, J. He et al., "Adaptive reclosing strategy for the mechanical DC circuit breaker in VSC-HVDC grid," Electric Power Systems Research, vol. 192, p. 107008, Mar. 2021.
[11] X. Pei, G. Tang, and S. Zhang, "Sequential auto-reclosing strategy for hybrid HVDC breakers in VSC-based DC grids," Journal of Modern Power Systems and Clean Energy, vol. 7, no. 3, pp. 633-643, May 2019.
[12] S. Xue, J. Lian, J. Qi et al., "Fault transient characteristic and adaptive reclosing technique of MMC-HVDC network," Power System Technology, vol. 42, no. 12, pp. 4015-4021, Dec. 2018.
[13] S. Zhang, G. Zou, B. Li et al., "Fault property identification method and application for MTDC grids with hybrid DC circuit breaker," International Journal of Electrical Power & Energy Systems, vol. 110, pp. 136-143, Sept. 2019.
[14] S. Yang, X. Xiang, X. Lu et al., "An adaptive reclosing strategy for MMC-HVDC systems with hybrid DC circuit breakers," IEEE Transactions on Power Delivery, vol. 35, no. 3, pp. 1111-1123, Jun. 2020.
[15] T. Wang, G. Song, and S. T. H. Kazmi, "Adaptive single-pole auto-reclosing scheme for hybrid MMC-HVDC systems," IEEE Transactions on Power Delivery, vol. 34, no. 6, pp. 2194-2203, Dec. 2019.
[16] Z. Li, J. Duan, W. Lu et al., "Pilot acceleration line protection of flexible MVDC distribution network," Automation of Electric Power Systems, vol. 45, no. 9, pp. 280-88, May 2021.
[17] J. Duan, Z. Li, Z. Wei et al., "A line accelerated protection scheme of flexible MVDC distribution system based on transient current derivative," Electrical Power System Research, vol. 183, p. 106269, Jun. 2020.
[18] Y. Yu, Y. Jin, Q. Jiang et al., "RT-LAB based modeling and simulation analysis of flexible DC distribution network," Power System Protection and Control, vol. 43, no. 19, pp. 125-130, Oct. 2015.
[19] B. Li, J. He, Y. Li et al., "High-speed directional pilot protection for MVDC distribution systems," International Journal of Electrical Power & Energy Systems, vol. 121, p. 106141, Oct. 2020.
[20] R. Song, J. Lu, and M. Zhang, "The Shanghai practice: improve the reliability of urban MV distribution system with K-station and its new network designs," in Proceedings of 25th International Conference on Electricity Distribution, Madrid, Spain, Jun. 2019, pp. 941-948.
[21] DC Distribution Voltage, T/CEC 107-2016, 2017.
[22] C. Zhang, G. Song, T. Wang et al., "Single-ended traveling wave fault location method in DC transmission line based on wave front information," IEEE Transactions on Power Delivery, vol. 34, no. 5, pp. 2028-2038, Oct. 2019.
[23] W. Xiang, S. Yang, L. Xu et al., "A transient voltage-based DC fault line protection scheme for MMC-based DC grid embedding DC breakers," IEEE Transactions on Power Delivery, vol. 34, no. 1, pp. 334-3454, Feb. 2019.
[24] B. Li, Y. Li, J. He et al., "A novel single-ended transient-voltage-based protection strategy for flexible DC grid," IEEE Transactions on Power Delivery, vol. 34, no. 5, pp. 1925-1937, Oct. 2019.

Zainan Li received the B.S. degree and the M.S. degree from Xi'an University of Technology, Xi'an, China, in 2017 and 2021, respectively, and he is currently pursuing the Ph.D. degree in North China Electric Power University, Beijing, China. His research interests include DC fault recovery and fault detection.

Jiandong Duan received the B.S. degree from Huazhong University of Science and Technology, Wuhan, China, in 1995, the M. S. degree from Guangxi University, Nanning, China, in 1998, and the Ph.D. degree from Xi'an Jiaotong University, Xi'an, China, in 2005, all in electrical engineering. He is currently a Professor with the Department of Electrical Engineering, Xi'an University of Technology, Xi'an, China. His research interests include power system analysis, DC distribution networks, distributed multi-en-

ergy system, relay protection, and smart grid monitoring technology.

Wenchao Lu received the B.S. degree in electrical engineering from Southwest Jiaotong University, Chengdu, China, in 2018. In 2021, he obtained the M.S. degree in electrical engineering from Xi'an University of Technology, Xi'an, China. At present, he is a Ph.D. student majoring in electrical engineering in Xi'an University of technology. His research interests include electromagnetic interference and relay protection.

Xiaotong Du received the B.S. degree from School of Electrical Engineering, Beijing Jiaotong University, Beijing China, in 2018. He is currently pursuing the M.Sc. degree in the School of Electrical Engineering, Xi'an University of Technology, Xi'an, China. His research interests include AC line protection and DC control of power system.

Wei Yang received the B.S. in electrical engineering from Xi'an University of Technology, Xi'an, China, in 2019, and will receive the M.S. degree in electrical engineering from Xi'an University of Technology, in 2022. His research interests include line protection for distribution network with DFIG, and circuit current characteristics of modular multilevel converter.

Siyu Tu received the B.S. and M.S. degrees in electrical engineering from Xi'an University of Technology, Xi'an, China, in 2018 and 2021, respectively. His research interests include optimal operation of integrated energy system, relay protection and transmission line.